Steel and Composite Structures, *Vol. 24, No. 6 (2017) 643-658*
DOI: https://doi.org/10.12989/scs.2017.24.6.643

Simplified criteria for finite element modelling of European preloadable bolts

Mario D'Aniello [*1], David Cassiano [2a] and Raffaele Landolfo [1b]

[1] *Department of Structures for Engineering and Architecture, University of Naples "Federico II", via Forno Vecchio, 36 – Napoli 80134, Italy*
[2] *ISISE, University of Coimbra, Polo II – R. Luís Reis Santos, 3030-788 Coimbra, Portugal*

(*Received August 09, 2016, Revised April 28, 2017, Accepted May 22, 2017*)

Abstract. High strength preloadable bolt assemblies are commonly adopted in beam-to-column bolted connections. Nowadays, two systems of high strength preloadable grade 10.9 bolt assembly are recommended in Europe for structural applications, namely HR and HV, which are characterized by different failure modes. Recently, experimental tests performed on HR and HV bolt assemblies highlighted that the type of bolt assembly may significantly influence the joint response. Therefore, the accuracy of numerical modelling of bolt assemblies is crucial to simulate effectively the non-linear behaviour of bolted joints with either failure mode 2 or mode 3 of the bolt rows. In light of these considerations, this present paper describes and discusses some modelling criteria for both HR and HV bolts to be implemented in 3D finite element models by finite element analysis and structural designers. The comparison between the calibrated models and experimental results shows the accuracy of the proposed assumptions in simulating all stages of assembly tensile response.

Keywords: high strength preloadable bolt; HR; HV; modelling criteria; bolted connections

1. Introduction

Bolted joints are widely adopted into steel structures, especially in Europe where they are typically characterised by lower constructional costs and simpler fabrication, erection and quality control procedures than those requested for welded connections (Da Silva and Santiago 2003). The EN 1993-1-8 (2005) provides a methodology based on the "Components Method", which allows to predict the response of beam-to-column joints, by breaking down the joint into its main mechanical components, that are subsequently characterized in terms of strength and stiffness. The behaviour of the bolt components described in EN 1993-1-8 (2005) is based on an elastic-perfectly plastic response and no distinction is made between the different types of bolt assemblies currently available in the European market.

In accordance with EN 1993-1-1 (2005) and EN 1090-1 (2008), two systems of high strength preloadable bolts can be adopted for structural applications in Europe, namely the HR (acronym for "High Resistance") system and the HV (German acronym for "Hochfeste Bolzen mit Vorspannung", meaning "high resistance bolts for pretension") system. The mechanical requirements as well as the bolt and nut assembly dimensions and tolerances for HR and HV systems are given in EN 14399-3 (2005) and EN 14399-4 (2005), respectively.

The typical failure mode of HR system is the shank necking (Prinz *et al.* 2014, D'Aniello *et al.* 2016), whereas the HV assemblies fail by thread-stripping and full removal of the nut (D'Aniello *et al.* 2016), as a consequence of thinner nuts and shorter threaded length tightened into the nut. The differences of both failure mode and corresponding inelastic tensile response can affect the strength and ductility of T-Stub connections (D'Aniello *et al.* 2016), also influencing the ultimate response of bolted joints under column loss scenario (Kwasnieswski 2010).

Several formulations and analytical models have been developed in the last decades for describing the tensile response of steel bolts. The modelling criteria proposed by Prinz *et al.* (2014), Swanson and Leon (2001) and Hanus *et al.* (2011) takes advantage of simple constitutive laws, which reduce computational effort, thus being suitable for both numerical and analytical analysis of bolted joints. However, it should be noted that these formulations were developed for North American bolt assemblies and generally do not account for the case of nut stripping and inelastic deformability of the threaded zone, thus being poorly accurate if implemented for European preloadable bolt assemblies (D'Aniello *et al.* 2016). On the other hand, FE modelling techniques using very refined meshing to model the thread geometry and surface interaction, as those adopted by Wu *et al.* (2012), Pavlovic *et al.* (2015), Grimsmo *et al.* (2016) and by Long *et al.* (2016), lead to very accurate results, but they significantly require high computational effort for calculating a single bolt assembly (generally unfeasible for ordinary computers and medium work-station platforms), due to the large number of finite elements and the convergence difficulties in computing complex contact interaction in the threaded zones.

Equivalent shank models were also proposed by Wu *et al.* (2012), but if the failure of bolt assemblies is the nut stripping, this type of equivalent shank model cannot

*Corresponding author, Ph.D., Assistant Professor,
E-mail: mdaniel@unina.it
[a] Ph.D. Student
[b] Ph.D., Professor

http://www.techno-press.org/?journal=scs&subpage=6
ISSN: 1229-9367 (Print), 1598-6233 (Online)

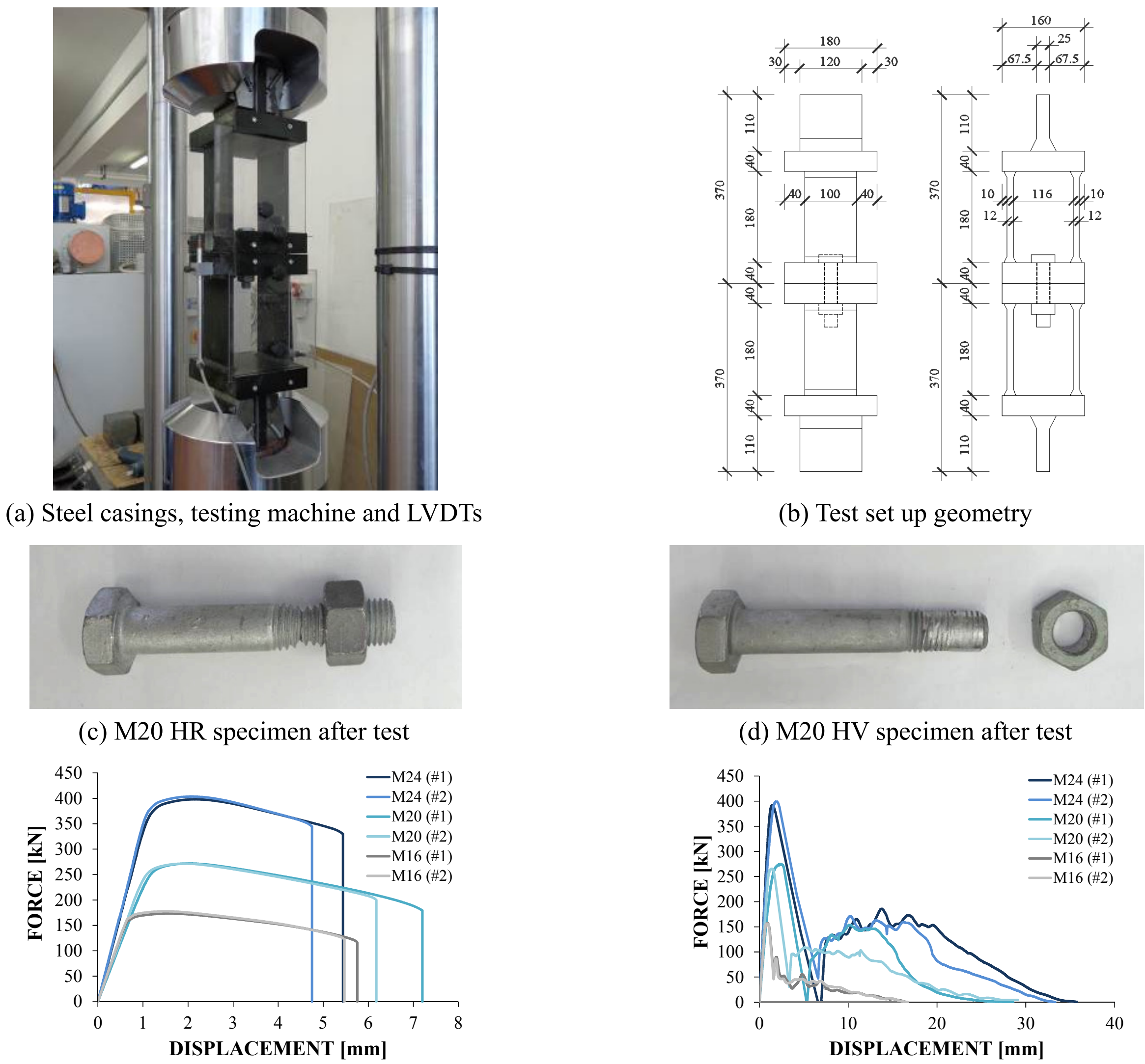

(a) Steel casings, testing machine and LVDTs

(b) Test set up geometry

(c) M20 HR specimen after test

(d) M20 HV specimen after test

(e) HR monotonic force-displacement curves

(f) HV monotonic force-displacement curves

Fig. 1 Experimental tests carried out by D'Aniello *et al*. (2016)

accurately reproduce the force-displacement response of the bolts in inelastic range. For the aforementioned reasons, it is effective and convenient to adopt FE modelling strategies for the bolt assembly that can simultaneously be accurate in describing the response of European preloadable bolts assemblies, as well as computationally time efficient. With this aim, modelling assumptions for simulating all stages of tensile response of both HR and HV bolt assemblies are presented and discussed in this paper. The article is organized in three main parts: (i) the first part describes the experimental results carried out to characterize the monotonic tensile behaviour of both HR and HV assemblies; (ii) in the second part the relevant modelling assumptions and their validations are described and discussed; (iii) in the third part the influence of the accuracy of bolt model on the response of T-Stub connections failing in mode 2 and mode 3 is shown.

2. Description of the experimental tests

The modelling criteria developed and described in this paper are validated against the experimental data obtained by the Authors in a former study (D'Aniello *et al*. 2016), where the monotonic tensile response of HR and HV assemblies was investigated varying the diameter (i.e., M16, M20 and M24).

The adopted test setup is shown in Fig. 1. In particular, the tension force was applied to the assemblies by means of test fixtures without inserts that were pulled using a universal electro-mechanical MTS testing machine (see Fig. 1(a)), as described in D'Aniello *et al.* (2016). The dimensions of the test set up are presented in Fig. 1(b). The bolt elongation was measured by two linear variable differential transformer (LVDT) characterized by a displacement range of ± 50 mm, which measured the relative displacement between the steel plates of the casings to which the assemblies were fastened. The difference in terms of failure mode between HR and HV assemblies can be recognized by comparing test specimens after failure (see Figs. 1(c)-(d)). As shown in Fig. 1(c), the failure of HR assemblies occurs by shank necking in the threaded shank zone (where the effective shank section is smaller). Instead, the failure mode for HV assemblies is nut stripping (see Fig. 1(d)). The comparison between an intact and a failed specimen highlights the smoothing of the crests in the threaded zone due to the nut removal.

Shank necking and nut stripping exhibit significantly different tensile force-displacement curves, as it can be observed by comparing the HR monotonic curves in Fig. 1(e) to the HV monotonic curves in Fig. 1(f). The response of HR assemblies is characterized by a linear elastic segment, followed by a nonlinear transition to the plastic domain and onset of softening from shank necking up to failure. Instead, the response of HV assemblies initially has a linear elastic segment followed by a very small plastic yielding branch. Afterwards, the assembly strength suddenly decreases due to first thread failure and it is maintained at about 30 to 40% of the peak strength in a residual strength plateau up to a very large displacement, after which strength decreases to zero upon full nut extraction.

The results from cyclic tests have also shown that the response curves and the failure modes of both bolt assemblies are not affected by the loading protocol (D'Aniello *et al*. 2016). Therefore, the numerical modelling criteria based on the monotonic tests are also effective under cyclic actions.

3. Finite element modelling criteria

The modelling of tensile response until failure of bolt assemblies is fundamental to ensure the accuracy of numerical results obtained by means of finite element analysis of steel bolted joints. Most of analytical and numerical studies proposed effective modelling assumptions for US bolt assemblies (Abel 1993, Sherbourne and Bahaari 1997, Barron and Bickford 1998, Swanson 1999, Mays 2000, Wade 2006). Recently, Prinz *et al*. (2014) proposed a trilinear stress-strain relationship to simulate the material behaviour of HR bolts used for bolted joints.

In the study by Prinz *et al*. (2014), the bolt ultimate strength is taken as 17% higher than the yield strength and the yield plateau extends indefinitely. The post-elastic transition branch is characterized by a slope equal to 0.0063E, being E the elastic modulus of the steel. However, the fact that the elastic branch presents a stiffness of 210 GPa indicates that the presented model pertains only to the shank deformability itself and does not account for other possible sources of deformability that contribute to the total assembly deformability, such as the threads. Since HV bolts are mostly dependent on deformations developing into the threaded zone of the shank, the numerical model should account for this additional source of deformability.

A refined multi-linear model for bolts was proposed by Swanson and Leon (2001), where the bolt response was derived from experimental tensile tests and schematized by four linear segments. The first simulates bolt behaviour prior to overcoming pre-tension force, the second segment represents the linear elastic response, the third segment models the onset of yielding (taken at 85% of the tensile capacity) and finally the fourth mimics the behaviour in plastic range. The elastic stiffness of the bolt K_b was computed according to Barron and Bickford (1998) and Swanson (1999) as follows

$$\frac{1}{K_b} = \frac{f \cdot d_b}{A_b \cdot E} + \frac{L_S}{A_b \cdot E} + \frac{L_{tg}}{A_b \cdot E} + \frac{f \cdot d_b}{A_{be} \cdot E} \tag{1}$$

where f is a correlation factor taken as 0.55; d_b is the nominal diameter of the bolt; A_b is the nominal area of the bolt shank; A_{be} is the effective area of the threads; L_s is the length of the bolt shank; L_{tg} is the length of the threaded portion included in the bolt's grip; E is the steel modulus of elasticity.

In order to avoid obtaining excessive values for the ultimate bolt elongation, this model limits elongation according to the following expression

$$\delta_{fract} = \frac{0.9 \cdot B_n \cdot L_S}{A_b \cdot E} + \varepsilon_{fract}\left(L_{tg} + 2/n_{th}\right) \tag{2}$$

where ε_{fract} is the fracture strain; B_n is the tensile capacity of the bolt; n_{th} is the number of threads per bolt unit length of the bolt.

The modelling approach by Swanson and Leon (2001) describes the most important stages of bolt response, allowing to capture accurately the softening due to the shank necking. More recently, Hanus *et al*. (2011) proposed a model to simulate also the bolt softening by using an equivalent force-displacement relationship in tension. This model is characterized by an elastic branch, a nonlinear transition segment and a bilinear descent branch.

A more refined approach was adopted by Pavlovic *et al*. (2015), which used a plasticity curve to define the hardening material behaviour, coupled with a damage initiation criterion and a damage evolution law to reproduce softening and failure. However, this procedure requires very detailed modelling of bolt assembly geometry, including the geometrical modelling of the treads on the shank and into the nut and the relevant surface interactions, thus requiring significant computational effort for the FE analysis of a single bolt. Therefore, unless required for a very specific and detailed application, the adoption of such a model is less convenient for quick and effective FE analysis of bolted joints. On the contrary, the use of a multi-linear constitutive law to simulate the bolt mechanical behaviour, when a sufficient number of segments is considered, can effectively describe all stages of bolt assembly response with a significant limitation of corresponding computational effort.

In order to highlight the accuracy of existing multi-linear models (N.B. early developed for US bolts) given by Abel (1993), Sherbourne and Bahaari (1997), Swanson (1999) and Mays (2000) to predict the behaviour of European high strength preloadable bolts, their force-displacement response curves obtained from both analytical and finite element analyses were compared to the corresponding experimental curves from D'Aniello *et al*. (2016) in Fig. 2(a), while Fig. 2(b) shows the comparison between results from finite element analyses incorporating models by these Authors and the experimental results from D'Aniello *et al*. (2016).

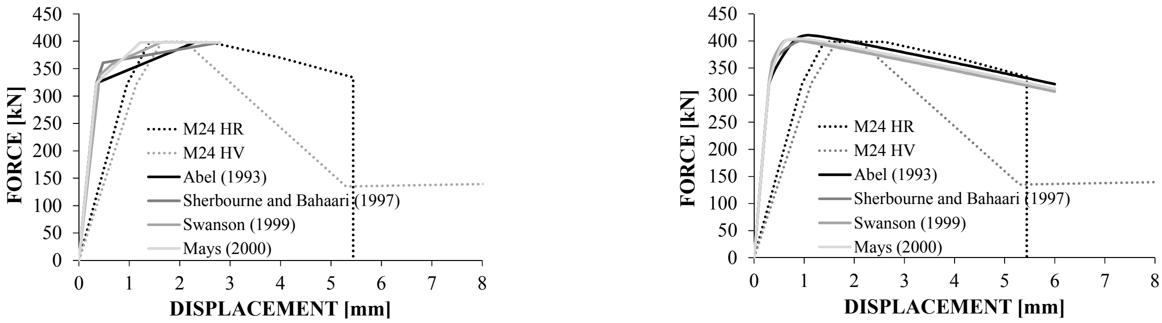

(a) Analytical response curves (b) Numerical response curves

Fig. 2 Comparison between the European piece-wise linear approximated response from tests carried out by D'Aniello *et al*. (2016) and modelling assumptions by Abel (1993), Sherbourne and Bahaari (1997), Swanson (1999) and Mays (2000) for M24 both HR and HV assemblies

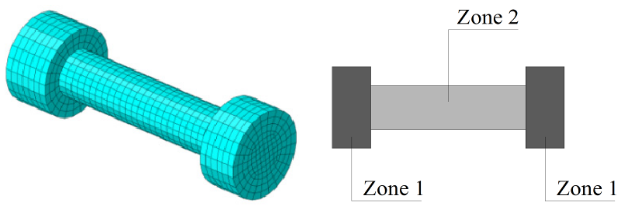

(a) Finite element model (b) Main components

Fig. 3 Model of HR assembly

As it can be observed, the examined formulations overestimate the initial stiffness of European bolt assemblies. This finding can be explained by considering that the threaded zones of EU bolts differ from US ones, which implies differences in terms of axial deformability. However, the modelling assumptions by Abel (1993), Sherbourne and Bahaari (1997), Swanson (1999) and Mays (2000) satisfactorily match the softening rate of HR assembly, while largely mispredict the post-yielding response of HV bolts. This comparison highlights that better refinement is necessary to accurately simulate European high strength bolts. Hence, in the following Sections, modelling assumptions with different levels of complexity and accuracy are proposed and verified against the presented experimental results.

3.1 Modelling of HR assemblies

3.1.1 Simplified model with equivalent shank

Finite element models of HR assemblies were carried out using Abaqus (Dassault 2014). The finite element type C3D8R (an 8-node linear brick type element with reduced integration and hourglass control) was used to discretize the model. In order to avoid shear locking and hourglass, more than three layers of finite elements across the thickness were adopted for all modelled parts of the bolts. The numerical analysis was conducted using a single step in which monotonically increasing displacements were imposed to the nut until reaching a target displacement corresponding to assembly failure. The equivalent geometry of HR bolts is made up of a single continuous element composed of two zones, as shown in Fig. 3(a), each of which characterized by different mechanical properties.

Both bolt head and nut (i.e., corresponding to Zone 1 as shown in Fig. 3(b) are modelled using a linear elastic material constitutive law with E = 210 GPa and Poisson coefficient v = 0.3. The shank (i.e., corresponding to zone 2 as shown in Fig. 3(b) was modelled by meshing a solid cylinder having the nominal circular gross area of the bolt, where the plastic behaviour of the assembly is concentrated.

Zone 2 should account for both elastic deformability of the shank and the plastic behaviour of the assembly, as well. The equivalent elastic modulus of the shank is calibrated

Table 1 HR and HV equivalent shank model elasticity modulus values

Bolt assembly type	Nominal diameter D	Smooth shank length L_{ss}	Threaded shank length L_{st}	Nominal shank area A_{nom}	Effective shank area A_{eff}	Stiffness smooth shank k_{ss}	Stiffness threaded shank k_{st}	Stiffness grip zone k_{tg}	Assembly stiffness $k_{Assembly}$	Equivalent elastic modulus E_{eq}	Equivalent elastic modulus from Eq. (1) $E_{Barron\&Bickford}$
	[mm]	[mm]	[mm]	[mm^2]	[mm^2]	[N/mm]	[N/mm]	[N/mm]	[N/mm]	[N/mm^2]	[N/mm^2]
HR	16	56.3	23.7	201	157	749965	1391139	1009579	328651	130766	157420
	20	61.0	19.0	314	245	1081532	2707895	697631	366659	93369	152080
	24	57.3	22.7	452	353	1657971	3265639	1355818	607191	107375	144196
HV	16	69.9	10.1	201	157	604049	3264356	511924	255411	101625	163259
	20	70.7	9.3	314	245	933146	5532258	386791	260568	66353	155945
	24	73.0	7.0	452	353	1301394	10440845	539119	367774	65118	149883

from the experimental curves, from which the stiffness of the assembly K_{eq} is subsequently derived.

Considering the smooth part of the shank, the threads and threaded portion included in the bolt's grip (i.e., the threads inside the nut) as a system of three springs working in series, the equivalent assembly stiffness can be computed as follows

$$\frac{1}{K_{eq}}=\frac{1}{K_{ss}}+\frac{1}{K_{st}}+\frac{1}{K_{tg}} \tag{3}$$

where the stiffness of the smooth part of the shank K_{ss} and the stiffness of the threaded part of the shank K_{st} are calculated on the basis of the theory of elasticity. The stiffness of the threads in the bolt grip K_{tg} can hence be derived by solving Eq. (3). Thus, rearranging Eq. (3) and expanding each term, the equivalent shank elastic modulus E_{eq} can be obtained as follows

$$E_{eq}=\left(\frac{1}{K_{ss}}+\frac{1}{K_{st}}+\frac{1}{K_{tg}}\right)^{-1}\times\frac{L_{ss}+L_{st}}{A_{nom}} \tag{4}$$

$$E_{eq}=\left(\frac{L_{ss}}{E_S A_{nom}}+\frac{L_{st}}{E_S A_{eff}}+\frac{1}{K_{tg}}\right)^{-1}\times\frac{L_{ss}+L_{st}}{A_{nom}} \tag{5}$$

where L_{ss} is the length of the smooth part of the shank and L_{st} is length of the threaded shank (as defined in D'Aniello *et al.* 2016); A_{nom} is nominal shank area; A_{eff} is effective shank area; E_S is the Young's modulus of the bolt steel.

The equivalent shank stiffness and elastic modulus for the examined HR and HV bolts (that have an L_{ss}+L_{st} length of the shank equal to 80 mm) are shown in Table 1, where it can be recognized that for both HR and HV bolts, the equivalent experimental elastic modulus E_{eq} is smaller than the elastic shank modulus $E_{Barron\&Bickford}$ computed according to Eq. (1).

The plasticity model was calibrated on the basis of monotonic tests by D'Aniello *et al.* (2016). The constitutive law to be applied to zone 2 is characterized by the multi-linear stress-strain curve shown in Fig. 4(a), and the coordinates of each point (i.e., P1 through P5) are computed according to Table 2. As it can be noted, the values of the maximum normalised stress ratio $\sigma_{true}/f_{y,k,bolt}$ (N.B. σ_{true} is the true stress that is defined as $\sigma_{true}=\sigma_{eng}(1+\sigma_{eng})$, being σ_{eng} and ε_{eng} the engineering stress and strain, respectively, while $f_{y,k,bolt}$ is the characteristic yield strength of the bolt) are around 1.0, being the shank modelled with its nominal diameter. By modelling the shank with its gross area, the true stress values are scaled down to simulate fictitiously the bolt strength. Softening is defined by a single segment between points P3 and P4. The ultimate plastic strain ε_{P4} is given from the quadratic interpolation curve of experimental results as shown in Fig. 4(b).

The comparison between the experimental and the calibrated numerical bolt force-displacement response curves is presented in Fig. 5, showing that the equivalent bolt shank model is capable of accurately reproducing all stages of the bolt response, including the softening associated to shank necking leading up to assembly failure.

3.1.2 Refined model with ductile damage

Also for the model with a ductile damage formulation (Dassault 2014), 3D solid finite element models were developed using Abaqus (Dassault 2014). The finite element type C3D8R was also adopted here using a mesh refinement similar to that described in the previous section (i.e., more than three layers of finite elements across the thickness for all modelled parts).

As for the equivalent shank model (See Section 3.1.1), the analysis was conducted by imposing monotonic displacements to the nut until reaching the failure of the assembly. Both initial stiffness and failure mode of HR bolts can be simulated using a more refined approach. With this regard, bolt geometry was also modelled with two different diameters along the shank, corresponding to

Table 2 Proposed constitutive law for HR equivalent shank

Point	$\varepsilon_{true,plastic}$	$\sigma_{true}/f_{y,k,bolt}$
[-]	[-]	[-]
P1	0.000	0.931
P2	0.005	0.988
P3	0.017	1.008
P4	-3.32E-3 D_{nom}^2 + 0.10709 D_{nom} - 0.453	$k_{softening}\,\varepsilon_{true,plastic,P4}$ + 1.0136
P5	ε_{P4} + 0.001	0.000
$k_{softening}$ = -0.3328		

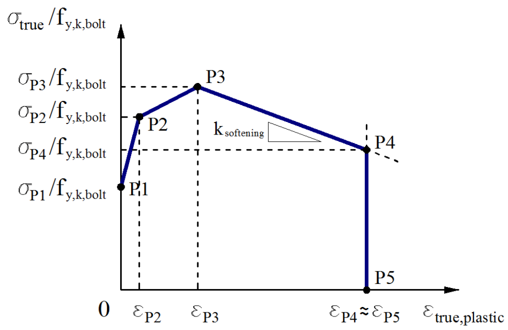

(a) Constitutive law

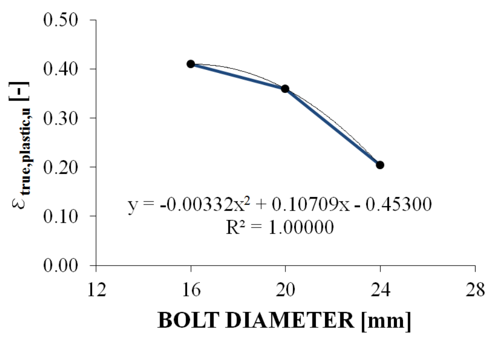

(b) Variation of ultimate strain with bolt diameter

Fig. 4 Proposed simplified constitutive law for HR equivalent bolt shank model

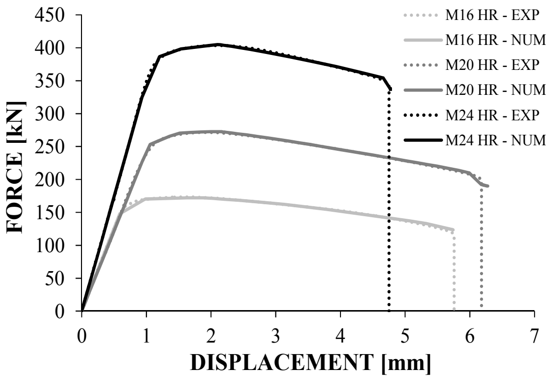

Fig. 5 Simplified model of HR bolts: comparison between experimental and finite element force-displacement response curves

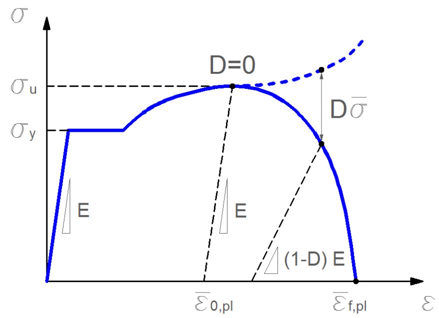

Fig. 6 Progressive ductile damage model

the smooth part and that corresponding to the equivalent area of the threads. This assumption allows directly obtaining the initial stiffness of the bolt with good accuracy. In addition, modelling the transition of diameter along the shank enforces the failure in the threaded zone as verified by experimental tests.

The ductile failure was simulated using progressive damage model (Dassault 2014), which accounts for damage initiation, softening, crack initiation and progression as shown in Fig. 6, where point D = 0 corresponds to the damage initiation point, the dashed curve represents the undamaged material response and the continuous line after point D = 0 represents the material softening. The formulation for ductile damage included in the Abaqus (Dassault 2014) software package was adopted, requiring the definition of the generic undamaged material response curve, damage initiation criterion and damage evolution law. The equivalent plastic strain at the onset of damage is dependent on strain rate and stress triaxiality T, defined as the ratio between the hydrostatic pressure stress (or isotropic stress) σ_H and the Von Mises equivalent stress σ_{eq} (Dassault 2014). The adopted undamaged material plasticity curve is the one given by Pavlovic *et al.* (2015) for grade 10.9 bolt assemblies. Fig. 7(a) shows the comparison between the adopted curve and those obtained by scaling the strength of the curves to account for the actual strength of the bolt specimens. As it can be recognized the differences are negligible, thus confirming the suitability of the data given by Pavlovic *et al.* (2015). Consistently, equal damage initiation criteria were adopted for the calibration of the M16, M20 and M24 assemblies. The curve of the adopted damage initiation criterion is shown in Fig. 7. A linear damage evolution law based was assumed, with the effective plastic displacement u^{pl} defined as the product of the equivalent plastic strain at failure ε_f^{pl} and of the characteristic length L of the finite element.

The calibrated curves for the damage parameter D as a function of u^{pl} are shown in Fig. 8(a), while the validated curves for the equivalent plastic strain at failure ε_f^{pl} as a function of bolt nominal diameter are shown in Fig. 8(b), having adopted the finite element length L = 2 mm. The calibrated curves show that the damage evolution is similar for different bolt diameters, consistently with the similar softening rates exhibited in experimental tests. Similar equivalent plastic displacement values were obtained for the M16 and M20 assemblies, while for the M24 a significant reduction was observed, coherently with the reduced ultimate displacement displayed in the experimental tests by D'Aniello *et al.* (2016).

The force-displacement comparison between the experimental and the calibrated numerical progressive damage model response is shown in Fig. 9(a) and the numerical model for the M24 assembly after fracture is presented in Fig. 9(b). The comparison between the M24 test specimen and the numerical model in Fig. 9(b) highlights that the fracture occurs in a similar position. This result shows that the adopted ductile damage model is capable of capturing the position of the fracture in a zone characterized by geometrical discontinuities and stress concentrations.

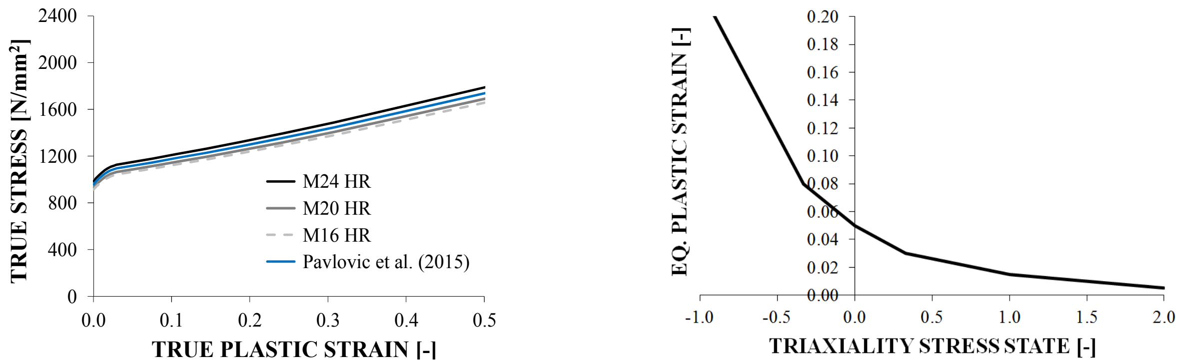

(a) Undamaged material constitutive law

(b) Damage initiation criterion (Pavlovic *et al.* 2015)

Fig. 7 Ductile damage model

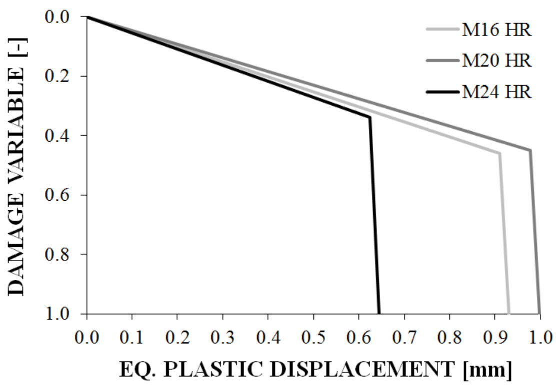

(a) Undamaged material constitutive law

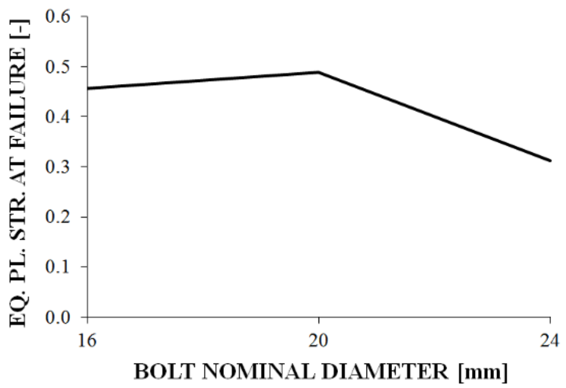

(b) Damage initiation criterion (Pavlovic *et al*. 2015)

Fig. 8 Ductile damage – calibrated parameters

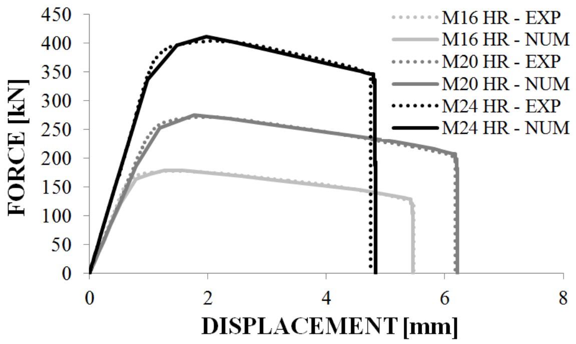

(a) Force-displacement response comparison

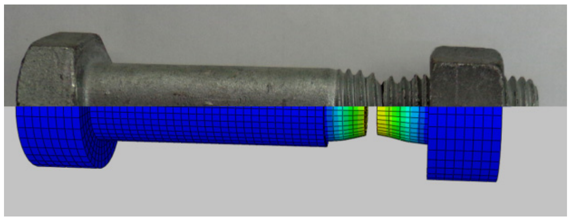

(b) M20 failed specimen and model after fracture

Fig. 9 Comparison between the predictions of ductile damage model and experimental results by D'Aniello *et al*. (2016)

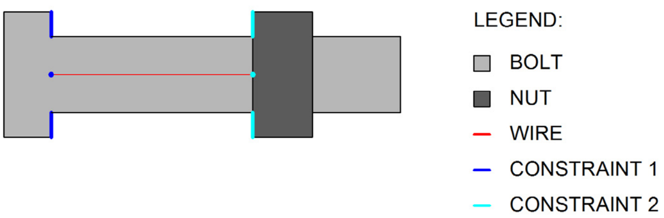

(a) Main components

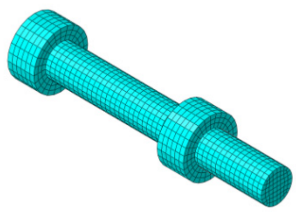

(b) Finite element model

Fig. 10 Model of HV assemblies

The calibrated progressive damage models are capable of accurately capturing damage initiation, softening and failure mode, although requiring a computational effort two times larger than the simplified model with equivalent shank (see Section 3.1.1). Hence, this modelling strategy appears to be suitable for application in small size models and to predict crack initiation and propagation patterns. For more complex models including a large number of bolt assemblies and for large scale parametric studies for which computational time is a key factor, a more simplified approach could be more advantageous.

3.2 Modelling of HV assemblies

The modelling assumptions described for HR bolts are not effective for HV assemblies, because their failure mode is characterized by the nut stripping that cannot be effectively simulated by an equivalent plastic failure as for the shank necking. However, modelling the thread-to-nut interactions requires significant computational effort. Hence, a simplified modelling strategy was proposed. The geometry of HV assembly was sub-structured into three main parts: (i) the nut modelled by solid finite elements; (ii) the bolt, comprising head and shank, modelled with solid finite elements; (iii) a fictitious one-dimensional wire finite element connected to the head and the nut as shown in Fig. 10(a) to simulate the nut stripping by means of an equivalent plastic behaviour. This choice allows over-coming problems of local shank necking by adopting a zero Poisson ratio value for the cross section of the wire element, to which a nonlinear material constitutive law function is assigned in order to account for the different stages of the HV assembly response.

As for HR assemblies, the geometry of the shank was

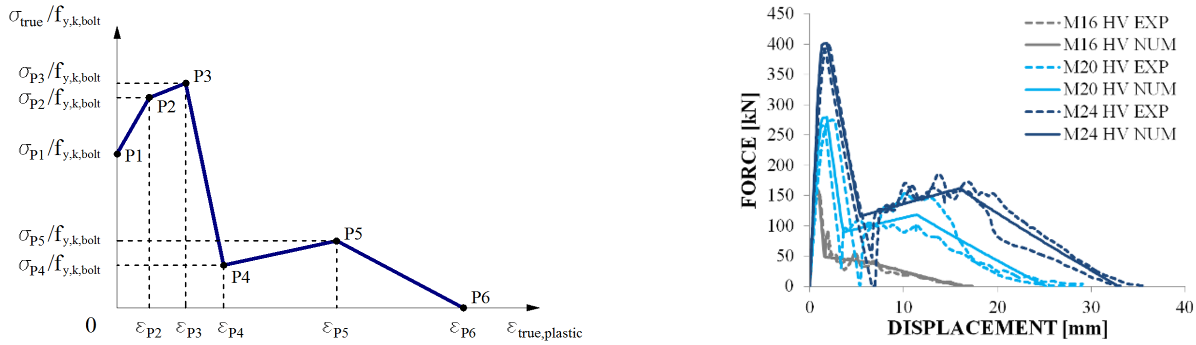

(a) Main components (b) Finite element model

Fig. 11 Proposed HV model

modelled by meshing a solid cylinder having the nominal circular gross area of the bolt. The nut geometry corresponds to a hollow cylinder with its internal diameter equal to the bolt nominal diameter. One end of the wire is connected to the nut through a rigid body constraint, which only allows longitudinal translation of the nut along the direction defined by the wire. In addition, the second end of the wire was connected to the internal surface of the bolt head by a rigid body constraint. Hard contact without friction was defined between the internal surface of the nut and the solid finite elements of the bolt shank, since all resistance opposing the nut slipping is accounted for in the constitutive law of the wire.

C3D8R finite elements were used for the solid parts of the model, which are characterized by a linear elastic behaviour with elastic modulus E = 210 GPa and Poisson coefficient ν = 0.3. The equivalent elastic modulus of the shank was determined as for HR assembly and the experimental and calculated values are reported in Table 1. Poisson coefficient equal to zero was associated to the wire element and its nonlinear behaviour consists in a multi-linear constitutive law that resists solely for tension relative displacements between the bolt head and the nut. The proposed equivalent multi-linear material response curve is derived on the stress-strain curves reported in D'Aniello *et al*. (2016) and shown in Fig. 11(a), while the equations of each segment are reported in Table 3. Although the proposed multi-linear material response curve requires the definition of six points, this constitutive law only depends on three geometrical parameters for one given bolt assembly, namely the bolt nominal diameter (D), the height of the nut (K) and to the threaded shank length outside the nut (Y), respectively. It should be also noted that the main advantage of this modelling strategy is that it can easily be implemented in 3D finite element simulations of steel bolted joints equipped with HV bolt assemblies. In order to capture the complex response curve due to nut stripping, the alternatives described in existing literature (e.g., Pavlovic *et al*. 2015, Long *et al*. 2016) would require to model in great detail the geometry of the crests of the threaded zone, thus requiring a very high number of additional finite elements in a very tight mesh to model this zone. Furthermore, all contact interactions between portions of failed crests and all surrounding elements would have to be defined, since the failed crests remain blocked inside the threaded nut zone, as experimentally observed by D'Aniello *et al*. (2016). This could make increase the computational efforts required to capture the strength loss and the post-peak response curve up to the complete extraction of the nut.

On the contrary, by using a wire element to model all stages of the bolt assembly response, the simulation of bolted joints with multiple rows of HV bolts can be made with very low computational effort, while satisfactory capturing all stages of the complex ultimate response of HV bolts. Of course, this proposed modelling approach should not be considered as the only adoptable method to simulate the behaviour of HV bolts, but it has to be considered as a viable alternative to simulate the complex ultimate response of this type of European pre-loadable bolts with relatively low computational effort.

The comparison between the experimental and the calibrated numerical bolt force-displacement response

Table 3 Proposed constitutive law for HV wire element

Point	$\varepsilon_{true,plastic}$	$\sigma_{true}/f_{y,k,bolt}$
[-]	[-]	[-]
P1	0	0.7867
P2	0.0023 α_1	0.9808 β_1
P3	0.0089 α_2	0.9878 β_2
P4	0.0502 α_3	0.2999 β_3
P5	$\varepsilon_{P4} + \alpha_4$	0.2999 $\beta_3 + \beta_4/f_{y,k,bolt}$ $(\varepsilon_{P5}-\varepsilon_{P4})$
P6	α_5	β_5

α_1 = 0.4 if D = 16; α_1 = 1.0 if D > 16
β_1 = 0.893 if D = 16 ; β_1 = 1.0 if D > 16
$\alpha_2 = \alpha_1$; $\beta_2 = \beta_1$; $\alpha_3 = 0.1091{*}D - 1.4$
$\beta_3 = -8.411E-3{*}D^2 + 3.431E-1{*}D - 2.443$
α_4 = 6.711E – 3*D - 4.585E-2
$\beta_4 = 1000{*}(-5.558E\text{-}2{*}D^2 + 2.406{*}D - 2.485E1)$
$\alpha_5 = 4.087E\text{-}4{*}(K+Y)^2 - 1.228E\text{-}2{*}(K+Y) + 2.825E\text{-}1$
$\beta_5 = 1E-4$
D ≡ Shank nominal diameter
K ≡ Height of the nut
Y ≡ Threaded shank length outside the nut
(as defined in D'Aniello *et al.* 2016)
D, K, Y in mm
$f_{y,k,bolt}$ ≡ bolt characteristic yielding stress

curves is presented in Fig. 11(b). Due to the variability of the experimental curves when nut stripping occurs, two monotonic experimental curves for each assembly diameter are plotted, so as to better verify the accuracy of the proposed modelling assumptions. The comparison displayed in Fig. 11(b) shows that the proposed modelling strategy is suitable for capturing the highly nonlinear behaviour of HV assemblies.

4. Verification of modelling assumptions against experimental tests on bolted joints

The accuracy of the proposed modelling criteria were also verified against some experimental results on bolted joints equipped with European pre-loadable bolts. It should be noted that, at the best knowledge of the Authors, the most of European tests available in literature were obtained using 8.8 grade bolts, whose mechanical features differ from those of HV and HR 10.9 grade assemblies. Therefore, the adopted experimental data came from existing studies available for the Authors, where either HR or HV bolts were used, namely: (1) tests carried out by Lima (2003) and Da Silva *et al*. (2004) on flush end-plate joints equipped with HR bolts and subjected to bending and axial force; (2) tests carried out by Ioan *et al*. (2016) on detachable shear links with bolted flush end-plate connections equipped with HV bolts; (3) monotonic test carried out by Landolfo (2016) on extended end-plate bolted joints equipped with HV bolts.

These specimens were used because their geometrical and mechanical properties were fully available. It should be noted that even though these connections did not failed in the bolts, their inelastic response is highly influenced by the behaviour of the bolts. For the sake of brevity, one specimen from each set of tests is shown hereinafter.

The finite element type C3D8R (an 8-node linear brick type element with reduced integration and hourglass control) was used to discretize all the solid parts of the model. The boundary conditions simulated the restraints imposed during the experimental tests. The interactions at the interfaces of elements in contact were defined considering a “Hard Contact” Normal Behaviour and the Tangential behaviour by means of Coulomb friction with the friction coefficient 0.3. In addition, dynamic implicit quasi-static analyses were performed.

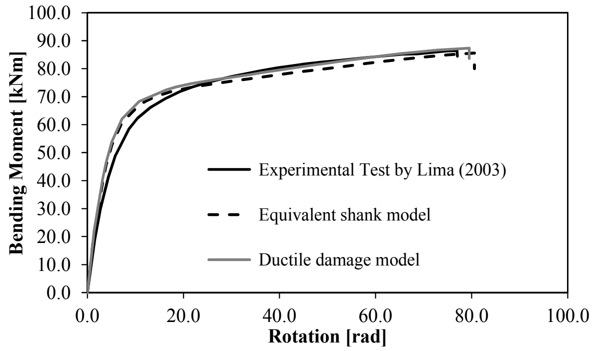

Fig. 13 Flush end-plate joint equipped with HR bolts: experimental vs. simulated response curve

4.1 Flush end-plate joints equipped with HR bolts

Lima (2003) and Da Silva *et al*. (2004) tested nine flush end-plate beam-to-column joints with the same configuration, but investigating several combinations of bending and compression axial forces. The columns (HEB 240) were simply-supported at both ends and the beams (IPE240) was restrained to avoid lateral torsional buckling. The end-plate was 15 mm thick, and all elements were made of steel grade S275. All bolts were M20 HR grade 10.9.

All tested specimens failed due to excessive plastic demand into either the end-plate or the welds. However, all bolts in tension developed plastic deformations. The comparison between the experimental failure mode of specimen subjected to bending only with the numerical predictions given by the simplified model (see Section 3.1.1) and the model with ductile damage (see Section 3.1.2) is shown in Fig. 12, which comprises the equivalent plastic strain (PEEQ) in the end-plate, the beam and in the bolts. The comparison between the experimental and predicted response curves is depicted in Fig. 13. As it can be observed, both modelling approaches provide satisfactory accuracy with very similar distribution of plastic strains. In addition, both models are able to simulate the prying effects developing into the upper bolt row, which are strongly dependent on the axial stiffness and carrying-capacity of bolts.

4.2 Detachable links with bolted flush end-plate connections equipped with HV bolts

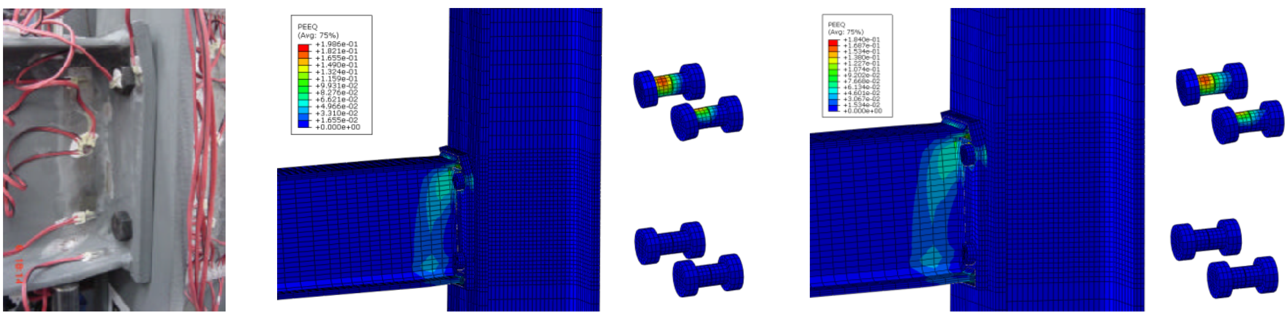

(a) (b) (c)

Fig. 12 Flush end-plate joint equipped with HR bolts: (a) experimental failure (Lima 2003); (b) simplified model with equivalent shank; (c) refined model with ductile damage

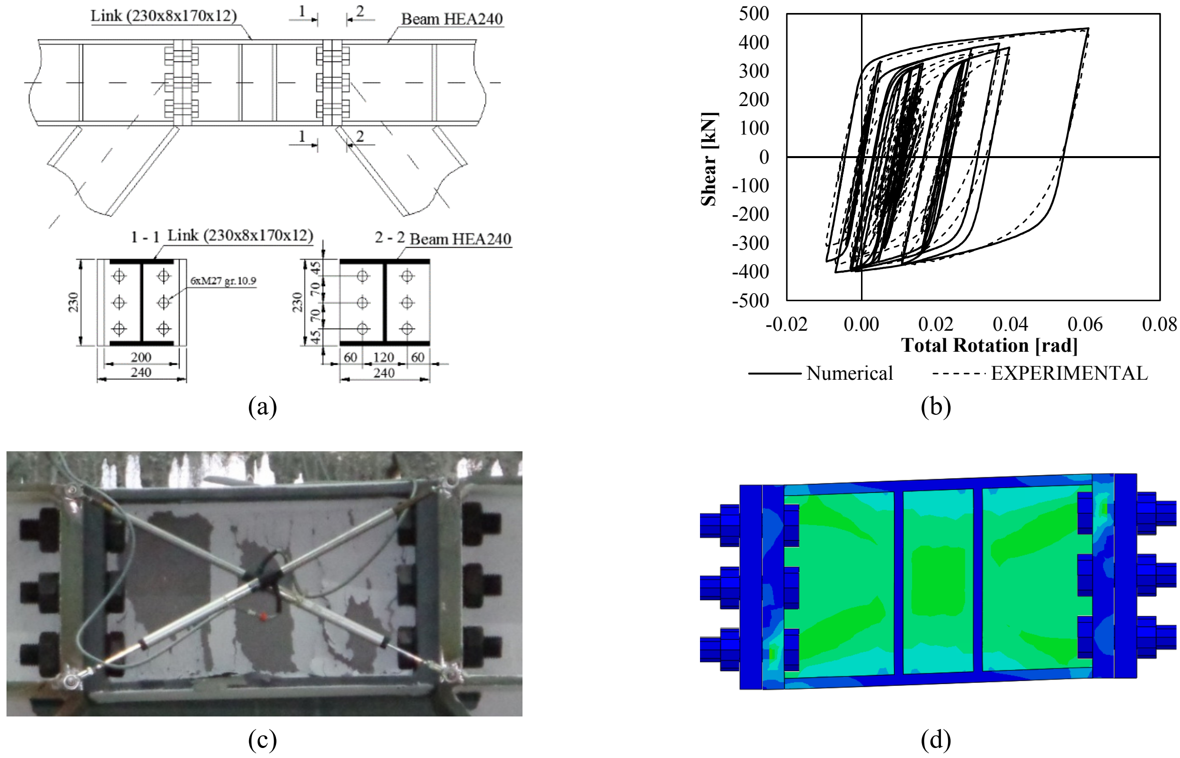

Fig. 14 Detachable links with connections equipped with HV bolts: (a) geometry; (b) experimental vs. simulated response curve; (c) experimental failure mode; (d) simulated failure mode

Ioan *et al*. (2016) tested detachable shear links within DUAREM project. The welded built up links (with web stiffeners welded only on one side) were made of S235 steel, while the end-plates (25 mm thick) were made of S355. All bolts were M27 HV grade 10.9. The geometry of the examined detachable links is depicted in Fig. 14(a).

Even though the bolts were not appreciably damaged during these tests, their role significantly influenced the overall response of the system. Indeed, in case of axial restraints at the ends of a shear link, as the case with detachable flush end-plate bolted connections, large catenary forces develop into the link, thus affecting the post-yield stiffness and the ultimate shear overstrength (Della Corte *et al*. 2013). Since, the axial stiffness of the bolts substantially influences the level of axial restraints at both link ends, the accuracy of the predicted post-yield stiffness of this type of shear link depends on the axial stiffness of the bolt assemblies. This consideration is also valid in case of joints subjected to catenary actions due to column loss (Cassiano *et al*. 2016, Tartaglia and D'Aniello 2017).

The behaviour of the bolts was simulated using the modelling approach described in Section 3.2. (see Table 3 for the constitutive law for HV wire element, which was updated considering the actual features of the bolts). The accuracy of the adopted modelling assumptions is shown in Figs. 14(b), (c) and (d), where the comparison between numerical and experimental results in terms of both shear force - rotation curves and failure mode highlights very good agreement. In particular, Fig. 14(d) shows the distribution of Von Mises stress into the bolts and the details of the equivalent wires connecting the nut and the head of the bolts. As it can be observed, the stress distributions into the shank, the head and the nut at each bolt row are consistent with the deformed shape.

4.3 Extended end-plate bolted joint equipped with HV bolts

Landolfo (2016) carried out a monotonic test an extended end-plate bolted joint equipped with HV bolts within the framework of EQUALJOINTS project (D'Aniello *et al*. 2017). The connection was designed to behave as partial strength with balanced column web panel, namely design to yield for the shear force corresponding to the bending resistance of the connection. The profiles and plates were made of S355 steel grade, while all the bolts were M27 HV grade 10.9. The column (HEB280) was simply supported at a distance equal to 3.4 m; the length of the beam (IPE360) was 3.4 m and additional restraints were provided in order to avoid its lateral-torsional buckling. The geometry of the examined extended end-plate bolted joint is depicted in Fig. 15(a).

As for the previous example, the behaviour of the bolts was simulated using the modelling approach described in Section 3.2. Figs. 15(b), (c) and (d) clearly show the accuracy of the finite element model. Indeed, the comparison between numerical and experimental response curve highlights excellent agreement in terms of initial and post-yield stiffness throughout the imposed displacement. The simulated failure mode satisfactory matches that experimentally observed, in terms of both connection opening and plastic deformation of column web panel. This outcome confirms that the model of the bolt is effective to

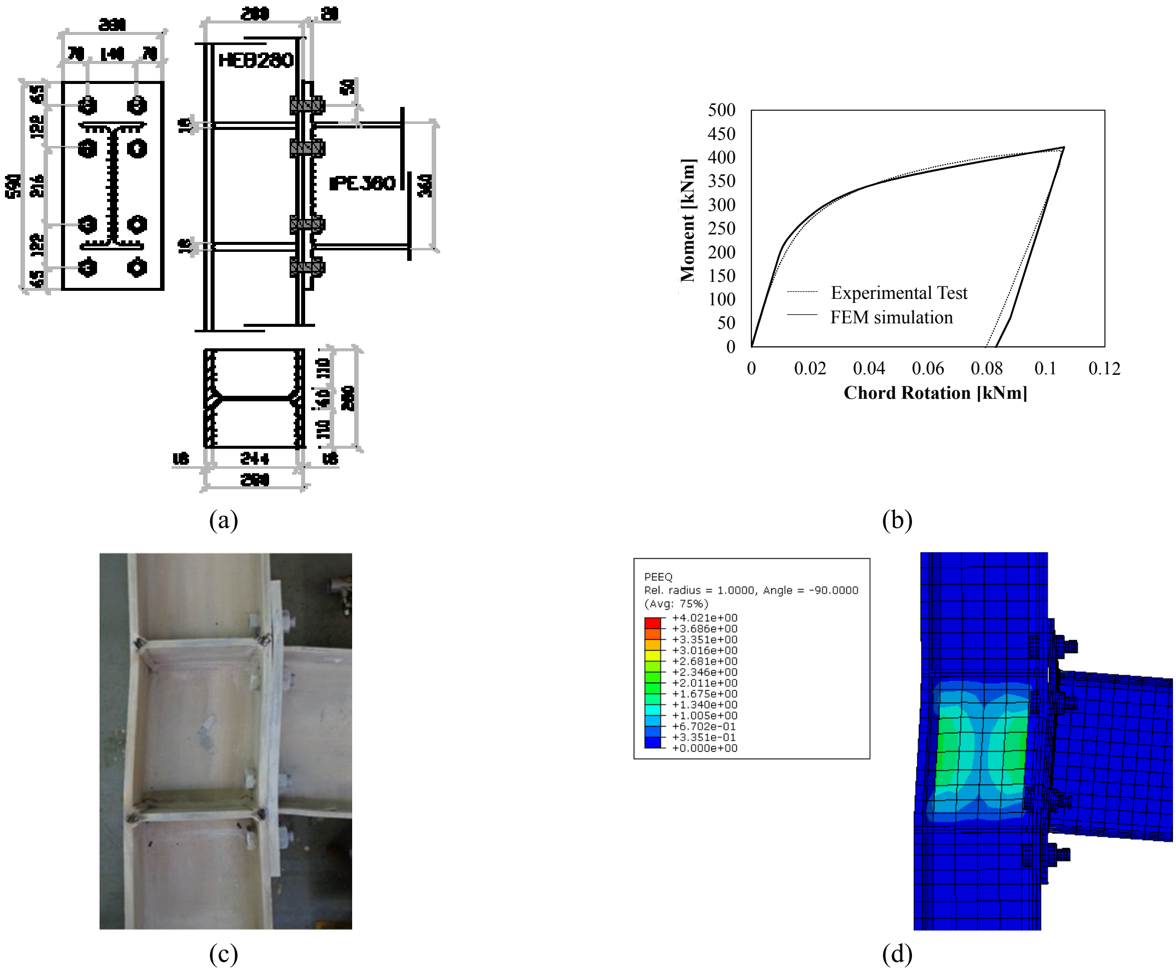

Fig. 15 Extended end-plate bolted joint equipped with HV bolts: (a) geometry; (b) experimental vs. simulated response curve; (c) experimental failure mode; (d) simulated failure mode

simulate the prying effects developing in the upper bolt rows from elastic to plastic stage.

5. Criticism of EC3 analytical prediction of T-Stub response with HR and HV assemblies

The T-stub is a widely used model to predict the behaviour of tension components in bolted joints. In case of T-Stub connections exhibiting either failure mode 2 or 3, the ultimate response is mostly influenced by the failure mode of the bolts, which differ from HR to HV assemblies. However, according to EC3:1-8 the analytical prediction does not depend on the type of bolts, but only on their resistance. Indeed, the bolts in tension are assumed as an elastic perfectly plastic component (Latour and Rizzano 2012, 2014, Latour *et al.* 2014, Francavilla *et al.* 2015, 2016). This assumption disregards the post-peak loss of strength that typically affects HV assemblies, while it can be consistent with the response of HR assemblies. The need of accounting for the strength loss of the bolt assemblies could be important even when the component method is used. Indeed, according to EN1993:1-8 the resistance of each bolt row of the connection derives from the internal equilibrium between the internal resultant of tension and compression forces. However, the distribution of those internal resultants varies with the connection rotation and the assumption of perfectly plastic resistance can be poorly accurate when mode 2 to 3 are activated. In order to highlight both the accuracy of EC3 analytical predictions and the differences on the T-stub response using HR or HV bolt assembly types, numerical FE models were developed on two T-Stub joints, whose geometry is depicted in Fig. 16(a), alternatively designed according to EN1993-1-8 to exhibit either mode 2 or mode 3. Only half T-stub was modelled, by taking advantage of symmetry conditions, as shown in ~~in~~ Fig. 16(b).

The analyses were carried out in a single step using dynamic implicit quasi-static analysis with a linear ramp function to apply displacements up to failure. Steel grade S355 with yield stress $fy = \gamma_{ov} \times f_{y,k} = 1.25 \times 355 = 444$ N/mm^2 (where γ_{ov} is the overstrength factor provided in EN 1998-1), is used for end-plate, column and beam. Contact was modelled using a Coulomb friction model with a friction coefficient equal to 0.3. Finite element type C3D8R was used to model all parts of the analysed T-stubs. The adopted bolt modelling techniques for HR and HV assemblies are those described in previously in Sections 3.1.2 and 3.2, respectively.

For the T-Stub with HV bolts the sudden transition from

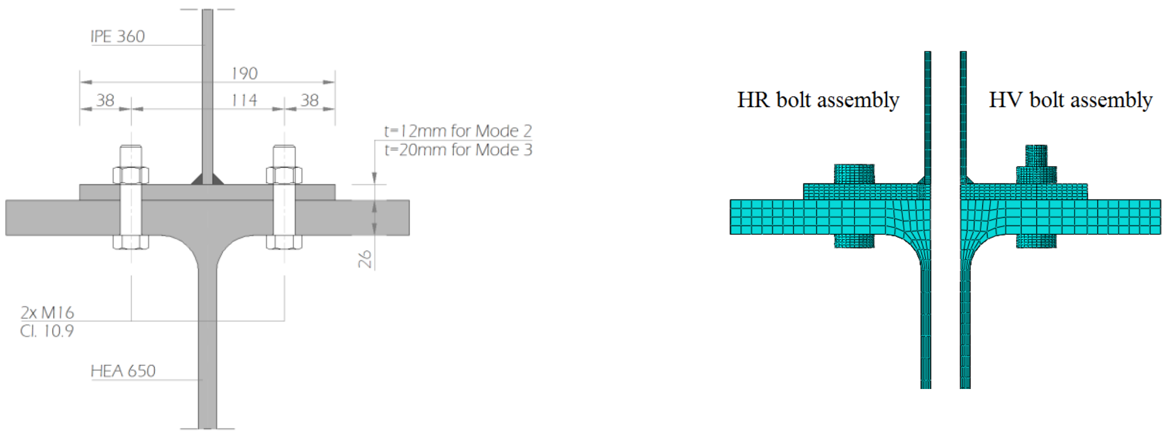

(a) Geometry (b) FE models for HR and HV cases

Fig. 16 Features of the T-stub models

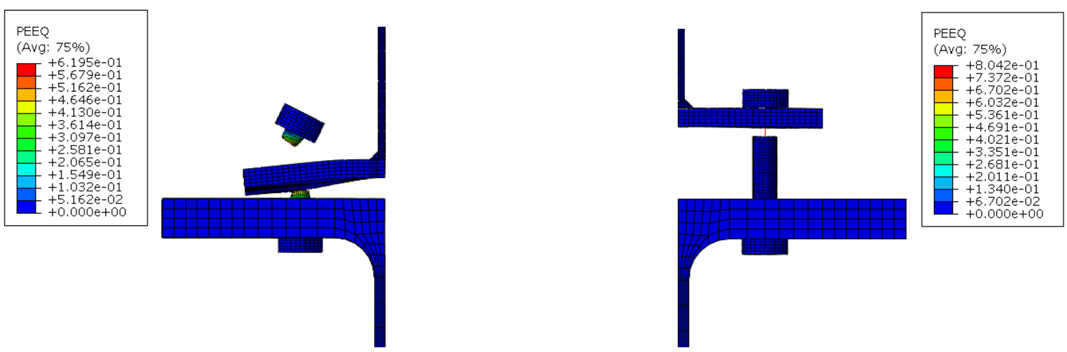

(a) HR failure mode (b) HV failure mode

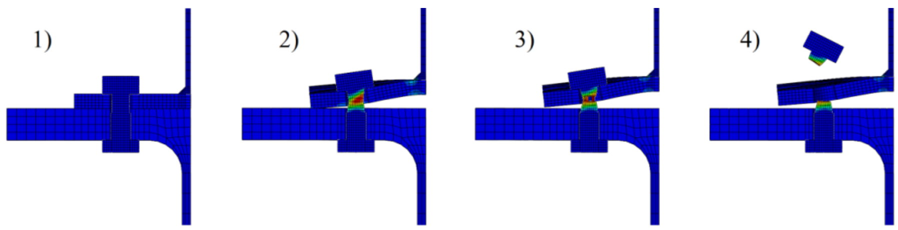

(c) Stages of failure mode for T-Stub with HR assembly – transversal view

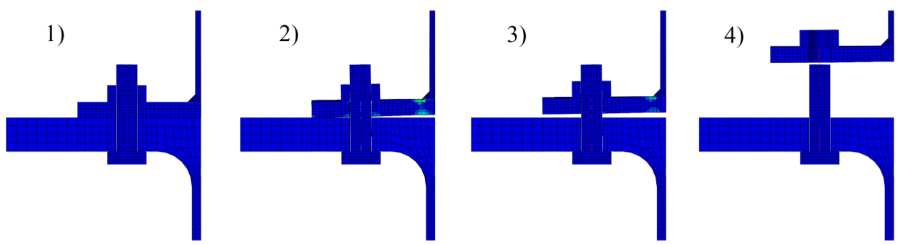

(d) Stages of failure mode for T-Stub with HV assembly – transversal view

Fig. 17 T-stub failure modesz

failure mode 2 to 3, which was predicted by the analytical model in D'Aniello *et al*. (2016), was found to introduce a pulse associated to the sudden loss of strength, which led to numerical difficulties and to some internal force fluctuation in the wire element. This computational problem can be overcome by reducing the degree of meshing in the wire element so as to limit the transverse vibration effects on the wire. This option did not lead to any loss of accuracy of the results, since the wire finite element is solely active in pure tension.

The failure modes for the T-Stubs designed for mode 2 with HR and HV assemblies are shown in Figs. 17(a) and (b) and the different stages leading up to failure of T-Stubs with HR and HV bolt assemblies are presented in Figs. 17(c) and (d).

For the case with HR bolts (see Fig. 17(c)), the T-Stub evolves in failure mode 2 up to bolt fracture, as predicted by the analytical model. Instead, the case with HV bolts exhibits a more complex behaviour as shown in Fig. 17(d), which starts with a failure mode 2 configuration for shank yield displacements (Stage 2) and subsequently evolves to mode 3-like (Stage 3) up to the complete extraction of the nut (Stage 4). Fig. 18(a) depicts the comparison between the numerical force-displacement response of T-Stub with HR bolts and the analytical prediction developed by D'Aniello *et al*. (2016), which used a 2D model with axially rigid plates and rigid-perfectly plastic end-plate in bending.

As it can be noted the simulated failure modes are consistent in terms of strength with the analytical mode 2 prediction. The EN 1993-1-8 prediction is also shown as a bi-linear model representing initial stiffness and strength capacity, assuming f_y = 444 N/mm^2 for members and the bolt ultimate stress from experimental tests.

A significant difference can be observed in terms of ultimate displacement for the HR case, which is due to several reasons. Indeed, the actual bending behaviour of the end-plate is not rigid-plastic, as assumed in the analytical model and likewise, the end-plate is not axially rigid as also assumed in the analytical model. This is consubstantiated by the fact that the end-plate strain hardening partially compensates for the bolt softening. Therefore, the numerical model shows smaller softening rate than the analytical curve for mode 2. Furthermore, as shown in Fig. 17(c), the nut rotates, implying that the bolt is not under pure tension as assumed in the analytical model, enabling the rotation of the end-plate. Finally, the Abaqus 3D model clearly shows that the deformed shape at failure differs from that assumed by the 2D analytical calculation. Indeed, finite element analysis displays that prior to bolt failure only the central part of the end-plate is in contact with the column flange. In addition, as observed in Stage 3 of Fig. 17(c), while bolt fracture is occurring the end-plate is no longer in contact with the column flange, implying prying forces equal to zero, hence reducing the demand on the bolt and enabling to achieve a larger displacement at collapse. In addition, the bending of end-plate edges contributes to reduce stiffness and to increase the ultimate displacement. Finally, the EN 1993-1-8 (2005) prediction overestimates the stiffness, while providing good agreement in terms of ultimate strength.

The comparison between numerical and analytical T-Stubs theoretically designed for mode 2 with HV assemblies is presented in Fig. 18(b). According to the analytical prediction, mode 2 is the failure mode up to a T-Stub displacement of 0.61 mm (to which corresponds a tensile force of 225 kN), after which mode 3 is activated. The FE response in Fig. 18(b) shows good agreement with the analytical prediction for mode 2. Also in this case, differences between FEM and analytical predictios are due to modelling assumptions, as previously described for the case with HR bolts. The loss of strength in the numerical model occurs at 2.4 mm displacement, after which the T-Stub transitions to failure mode 3, as recognisable by the correspondence in terms of strength with the mode 3 analytical curve. For the T-Stub with HV assemblies, the transition to mode 3 leads to a better agreement with the analytical predictions, since end-plate strain hardening, nut rotation and partial end-plate contact with the column flange do not occur to the same extent as in mode 2 failure. The ultimate displacement for the FE model is higher than mode 2 prediction mostly due to difference in terms of initial stiffness. As for HR bolts, the EN 1993-1-8 (2005) prediction overestimates initial stiffness and does not account for strength reduction leading to potentially unsafe predictions of T-Stub response.

In order to assess the T-Stub response in mode 3 with the proposed HR and HV modelling criteria, other two FE models were developed based on the geometry shown in Fig. 16(a), but with an end-plate thickness equal to 20 mm. The FE models are shown in Figs. 19(a) and (b). The comparison in terms of force-displacement response curves between analytical and numerical T-Stub models with HR assemblies is presented in Fig. 19(c), where the numerical model clearly displays lower stiffness and larger displacement at failure. As for the former cases designed for mode 2, the difference of initial stiffness is due to the end-plate that is not perfectly rigid as assumed by the analytical model. Furthermore, finite element models exhibit the yielding of welds and end-plate, which also contribute to reduce the stiffness.

This result is also in line with the experimental results on end-plate beam-to-column joints (e.g., Broderick and Thompson 2002, Aribert *et al.* 2004, Girão Coelho and Bijlaard 2007, etc.), which showed that EN 1993-1-8 (2005) can significantly overestimate the initial stiffness of bolted joints. Since the bolts are key components to determine

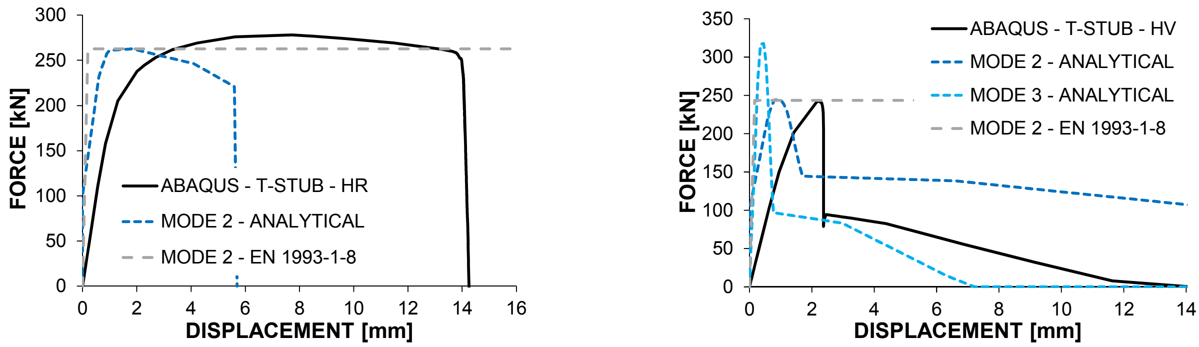

(a) T-Stub with HR assemblies (b) T-Stub with HV assemblies

Fig. 18 Force-displacement comparison between numerical model and analytical models from D'Aniello *et al*. (2016)

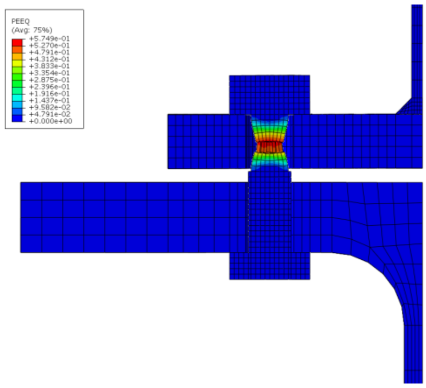

(a) Failure mode for T-Stub with HR assembly

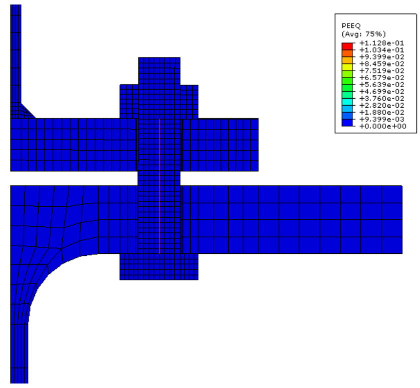

(b) Failure mode for T-Stub with HV assembly

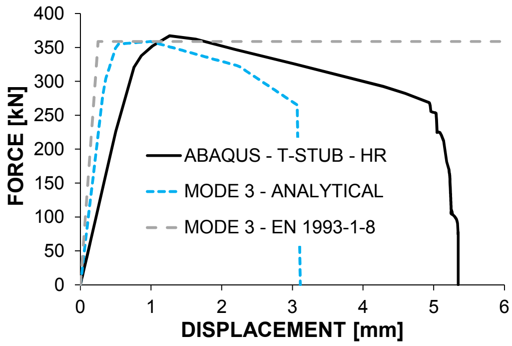

(c) Response for T-Stub with HR assembly

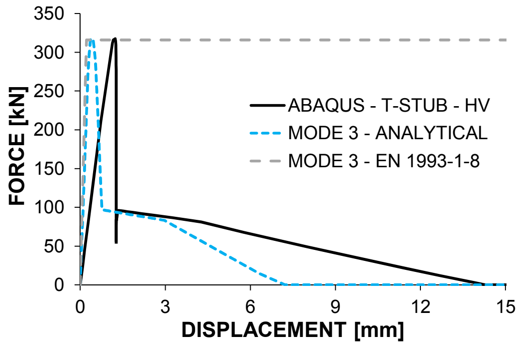

(d) Response for T-Stub with HV assembly

Fig. 19 T-Stub models with mode 3 failure – failure modes and comparison to analytical prediction model by D'Aniello *et al.* (2016)

joint stiffness, these considerations highlight that the formulation for the stiffness coefficient of bolts in tension provided by EN 1993-1-8 (2005) should be revised in order to account for the type of bolt assembly.

6. Conclusions

Modelling criteria for European preloadable grade 10.9 HR and HV bolts are described and discussed in this paper.

Two alternative modelling strategies with different levels of complexity and refinement are proposed for HR bolt assemblies, namely (i) the simplified equivalent shank model; and (ii) the refined ductile damage model. The comparison with test results shows that both proposed modelling approaches can accurately simulate all stages of bolt assembly response, including elastic response, plasticity onset, softening and initiation of failure. However, the failure mode with shank necking can be solely simulated by means of the refined ductile damage model.

The proposed modelling criteria for HV bolt assemblies are conceived to simulate the nut stripping without simulating the geometry of the threads and the contact interactions with the nut. In particular, the thread-stripping is obtained using a one-dimensional wire type finite element with Poisson coefficient equal to zero and characterized by a multi-linear behaviour curve calibrated on the experimental response of HV assemblies in order to mimic the elastic response, the plastic onset, the initial thread failure with significant strength reduction, the residual strength plateau and the final softening up to the nut removal.

The accuracy of the proposed modelling criteria was also verified against some experimental results on connections equipped with either HR or HV bolts.

The accuracy of EC3:1-8 analytical prediction of failure mode 2 and 3 of T-Stub connections with both HR and HV assemblies is also discussed and the comparison between the numerical simulations highlight the need to account for the type of bolt assembly even analytically. In particular, the comparison between analytical and finite element model of T-Stubs with HR bolts shows good agreement in terms of strength but significant differences in terms of initial stiffness and ultimate displacement, thus highlighting that the formulation for the stiffness coefficient of bolts in tension given in EN 1993-1-8 (2005) needs to be improved.

The comparison between analytical and numerical models of T-Stubs with HV bolts showed that EN 1993-1-8 (2005) does not accurately predict the strength and the displacement capacity of the assembly, thus being potentially non-conservative. These results highlight the need to revise the current version of EN1993-1-8, by distinguishing between HV and HR bolts and relating the strength and ductility of bolt components to the each typology of bolt assembly.

It is important to highlight that the proposed modelling assumptions should be intended as an attempt to develop finite element models able to mimic the force-displacement response of European preloadable grade 10.9 HR and HV bolts with limited computational effort. Of course, the findings of this study do not have the presumption to cover all possible types of bolts and mechanical fasteners available on the constructional market, being also out of its scope. Therefore, the extension of the presented results to other types of bolt assemblies will need specific investigation.

Acknowledgments

The research leading to these results has received funding from the European Union's Research Fund for Coal and Steel (RFCS) research programme under grant agreement n° RFSR-CT-2013-00021.

The Authors thank also the financial support of the RELUIS project "Linea di Ricerca Acciaio & Composte Acciaio-Calcestruzzo" 2014-2015.

References

Abel, M.S.M. (1993), "Four-bolt extended unstiffened moment end-Plate connections", M.Sc. Dissertation; Virginia Polytechnic Institute and State University Blacksburg, Blacksburg, VA, USA.

Aribert, J., Braham, M. and Lachal, A. (2004), "Testing of simple joints and their characterization for structural analysis", *J. Const. Steel Res.*, **60**(3), 659-681.

Barron, J. and Bickford, J.H. (1998), *Handbook of Bolts and Bolted Joints: Computing the strength of a fastener*, Marcel Dekker, New York, NY, USA.

Broderick, B.M. and Thompson, A.W. (2002), "The response of flush end-plate joints under earthquake loading", *J. Const. Steel Res.*, **58**(9), 1161-1175.

Cassiano, D., D'Aniello, M., Rebelo, C., Landolfo, R. and da Silva, L. (2016), "Influence of seismic design rules on the robustness of steel moment resisting frames", *Steel Compos. Struct., Int. J.*, **21**(3), 479-500.

D'Aniello, M., Cassiano, D. and Landolfo, R. (2016), "Monotonic and cyclic inelastic tensile response of European preloadable GR10. 9 bolt assemblies", *J. Const. Steel Res.*, **124**, 77-90.

D'Aniello, M., Tartaglia, R., Costanzo, S. and Landolfo, R. (2017), "Seismic design of extended stiffened end-plate joints in the framework of Eurocodes", *J. Const. Steel Res.*, **128**, 512-527.

Da Silva, L.S. and Santiago, A. (2003), *Manual de Ligações Metálicas*, CMM – Associação Portuguesa de Estruturas Metálicas e Mistas.

Da Silva, L.S., Lima, L., Vellasco, P. and Andrade, S. (2004), "Behaviour of flush end-plate beam to column joints under bending and axial force", *Steel Compos. Struct., Int. J.*, **4**(2), 77-94.

Dassault (2014), Abaqus 6.14 - Abaqus Analysis User's Manual, Dassault Systèmes Simulia Corp.

Della Corte, G., D'Aniello, M. and Landolfo, R. (2013), "Analytical and numerical study of plastic overstrength of shear links", *J. Const. Steel Res.*, **82**, 19-32.

EN 1090-1 (2008), Execution of steel structures and aluminium structures - Part 1: Requirements for conformity assessment of structural components, Brussels, Switzerland.

EN 1993-1-1 (2005), Eurocode 3 - Design of steel structures - Part 1-1: General rules and rules for buildings, Brussels, Switzerland.

EN 1993-1-8 (2005), Eurocode 3 - Design of steel structures - Part 1-8: Design of joints, Brussels, Switzerland.

EN 1998-1 (2004), Eurocode 8 - Design of structures for earthquake resistance - Part 1: General rules, seismic actions and rules for buildings, Brussels, Switzerland.

EN 14399-3 (2005), High strength structural bolting for preloading - Part 3: System HR - Hexagon bolt and nut assemblies, Brussels, Switzerland.

EN 14399-4 (2005), High strength structural bolting for preloading - Part 4: System HV - Hexagon bolt and nut assemblies, Brussels, Switzerland.

Francavilla, A.B., Latour, M., Piluso, V. and Rizzano, G. (2015), "Simplified finite element analysis of bolted T-stub connection components", *Eng. Struct.*, **100**, 656-664.

Francavilla, A.B., Latour, M., Piluso, V. and Rizzano, G. (2016), "Bolted T-stubs: A refined model for flange and bolt fracture modes", *Steel Compos. Struct., Int. J.*, **20** (2), 267-293.

Girão Coelho, A.M. and Bijlaard, F. (2007), "Experimental behaviour of high strength steel end-plate connections", *J. Const. Steel Res.*, **63**(9), 1228-1240.

Grimsmo, E.L., Aalberg, A., Langseth, M. and Clausen, A.H. (2016), "Failure modes of bolt and nut assemblies under tensile loading", *J. Const. Steel Res.*, **126**, 15-25.

Hanus, F., Zilli, G. and Franssen, J.M. (2011), "Experimental tests and analytical models for welds and grade 8.8 bolts under heating and subsequent cooling", *J. Struct. Fire Eng.*, **2**(3), 181-194.

Ioan, A., Stratan, A., Dubina, D., Poljansek, M., Molina, F.J., Taucer, F., Pegon, P. and Sabau, G. (2016), "Experimental validation of re-centering capability of eccentrically braced frames with removable links", *Eng. Struct.*, **113**, 335-346.

Kwasnieswski, L. (2010), "Nonlinear dynamic simulations of progressive collapse for a multistory building", *Eng. Struct.*, **32**(5), 1223-1235.

Landolfo, R. (2016), "European qualification of seismic resistant steel bolted beam-to-column joints: The Equaljoints project", *Proceedings of 1st EU-Sino Workshop on Earthquake-Resistance of Steel Structures*, Shanghai, China, October.

Latour, M. and Rizzano, G. (2012), "Experimental behavior and mechanical modeling of dissipative T-stub connections", *J. Struct. Eng.*, **138**(2), 170-182.

Latour, M. and Rizzano, G. (2014), "Experimental analysis on the cyclic response of beam to column joints: State-of-the-art at Salerno University", *Op. Constr. Build. Tech. J.*, **8**(1), 227-247.

Latour, M., Rizzano, G., Santiago, A. and Da Silva, L. (2014), "Experimental analysis and mechanical modeling of T-stubs with four bolts per row", *J. Const. Steel Res.*, **101**, 158-174.

Lima, L. (2003), "Comportamento de ligações com placa de extremidade em estruturas de aço submetidas a momento fletor e força axial", Ph.D. Thesis; Pontifícia Universidade Católica do Rio de Janeiro, Rio de Janeiro, Brazil.

Long, L., Yan, Y., Gao, X. and Kang, H. (2016), "Three-dimensional finite element simulation and application of high-strength bolts", *Steel Compos. Struct., Int. J.*, **20**(3), 501-512.

Mays, T.W. (2000), "Application of the finite element method to the seismic design and analysis of large moment end-plate connections", Ph.D. Dissertation; Virginia Polytechnic Institute and State University, Blacksburg, VA, USA.

Pavlovic, M., Heistermann, C., Veljkovic, M., Pak, D., Feldmann, M., Rebelo, C. and Silva, L.S. (2015), "Connections in towers for wind converters, part I: Evaluation of down-scaled experiments", *J. Const. Steel Res.*, **115**, 445-457.

Prinz, G.S., Nussbaumer, A., Borges, L. and Khadka, S. (2014), "Experimental testing and simulation of bolted beam-column connections having thick extended endplates and multiple bolts per row", *Eng. Struct.*, **59**, 434-447.

Sherbourne, A.N. and Bahaari, M.R. (1997), "Finite element prediction of end plate bolted connection behavior. I: Parametric study", *J. Struct. Eng.*, **123**(2), 157-164.

Swanson, J.A. (1999), "Characterization of the strength, stiffness, and ductility behavior of t-stub connections", Ph.D. Dissertation; Georgia Institute of Technology, Atlanta, GA, USA.

Swanson, J. and Leon, R. (2001), "Stiffness modelling of bolted t-stub connection components", *J. Struct. Eng.*, **127**(5), 498-505.

Tartaglia, R. and D'Aniello, M. (2017), "Nonlinear performance of extended stiffened end plate bolted beam-to-column joints subjected to column removal", *Open Civil Eng. J.*, **11**, 3-15.

Wade, P.M. (2006), "Characterization of high-strength bolt behavior in bolted moment connections", M.Sc. Dissertation; North Carolina State University, Raleigh, NC, USA.

Wu, Z., Zhang, S. and Jiang, S-F. (2012), "Simulation of Tensile Bolts in Finite Element Modeling of Semi-rigid Beam-to-column Connections", *Int. J. St. Struct.*, **12**(3), 339-350.

CC